



HAL
open science

A comparison of Forbush Decreases driven by ICMEs and SIRs

C. Gutierrez, S. Dasso, P. Démoulin, M. Janvier

► **To cite this version:**

C. Gutierrez, S. Dasso, P. Démoulin, M. Janvier. A comparison of Forbush Decreases driven by ICMEs and SIRs. *Journal of Atmospheric and Solar-Terrestrial Physics*, 2024, 259, pp.106232. 10.1016/j.jastp.2024.106232 . obspm-04595711

HAL Id: obspm-04595711

<https://hal-obspm.ccsd.cnrs.fr/obspm-04595711>

Submitted on 31 May 2024

HAL is a multi-disciplinary open access archive for the deposit and dissemination of scientific research documents, whether they are published or not. The documents may come from teaching and research institutions in France or abroad, or from public or private research centers.

L'archive ouverte pluridisciplinaire **HAL**, est destinée au dépôt et à la diffusion de documents scientifiques de niveau recherche, publiés ou non, émanant des établissements d'enseignement et de recherche français ou étrangers, des laboratoires publics ou privés.

A comparison of Forbush Decreases driven by ICMEs and SIRs

C. Gutierrez^{a,*}, S. Dasso^{a,b}, P. Démoulin^{c,d} and M. Janvier^{e,f,d}

^aCONICET, Universidad de Buenos Aires, Instituto de Astronomía y Física del Espacio, Grupo LAMP, Godoy Cruz 2290, Ciudad Autónoma de Buenos Aires, 1428, Buenos Aires, Argentina

^bUniversidad de Buenos Aires, Facultad de Ciencias Exactas y Naturales, Departamento de Ciencias de la Atmósfera y los Océanos, Grupo LAMP, Intendente Güiraldes 2160 Ciudad Universitaria, Buenos Aires, 1428, Buenos Aires, Argentina

^cLESIA, Observatoire de Paris, Université PSL, CNRS, Sorbonne Université, Université Paris Cité, 5 place Jules Janssen, Meudon 92195, France

^dLaboratoire Cogitamus, rue Descartes, Paris 75005, France

^eEuropean Space Agency, ESTEC, Noordwijk, The Netherlands

^fUniversité Paris-Saclay, CNRS, Institut d'Astrophysique Spatiale, Orsay, Paris 91405, France

ARTICLE INFO

Keywords:

Cosmic rays
Solar coronal mass ejections
Solar wind

ABSTRACT

Solar wind structures passing Earth can shield Earth from Galactic Cosmic Rays (GCRs), producing variations in the GCR flux that can be observed by ground-based detectors. In this paper we study the differences of Forbush decreases (FDs) produced by Interplanetary Coronal Mass Ejections (ICMEs) and Stream Interaction Regions (SIRs), applying a superposed epoch technique to large samples of FDs associated with ICMEs and SIRs. The analysis of the GCRs flux is made using data from neutron monitors at an Antarctic station (McMurdo). We also study the dependence of the FD properties with the bulk velocity of ICMEs/SIRs. We confirm that the faster ICMEs cause the largest FDs. In contrast, the FD intensity in SIRs is weakly dependent of the bulk velocity. Indeed, we find that ICMEs and SIRs with similar solar wind velocity produce very different FDs. This points for a dominant role of the magnetic field in screening GCRs. Finally, we find that in ICMEs the minimum GCR flux is usually observed close to the beginning of the magnetic ejecta, while in SIRs this is usually at the trailing edge.


1. Introduction

Galactic Cosmic Rays (GCRs) are high energy particles of galactic origin that penetrate the solar system. The transport of these GCRs through magnetic fields was first described by Parker (1965). GCRs are modulated by the advection of the solar wind, cross magnetic field diffusion, drifts of the particles, and adiabatic energy changes. The long term variability of GCRs has an anti-correlation with the solar activity (sunspot) cycle (Usoskin, Kananen, Mursula, Tanskanen and Kovaltsov, 1998, and references therein). Short term depressions are also observed due to structures in the interplanetary medium such as interplanetary coronal mass ejections (ICMEs) and stream interaction regions (SIRs).

ICMEs are the interplanetary counterpart of coronal mass ejections (e.g., Richardson and Cane, 2010; Rouillard, 2011). They consist of magnetized plasma released from the solar corona. Initially, they are magnetically closed structures with their footpoints connected to the Sun. As ICMEs propagate in the interplanetary medium they expand as a consequence of an imbalance between the internal forces and the decrease with distance from the Sun of the total pressure at the ICME boundary (Démoulin, Nakwacki, Dasso and Mandrini, 2008; Démoulin and Dasso, 2009). A large fraction of ICMEs produce interplanetary shocks due to their velocity being larger than the magnetosonic speed in the reference frame of solar wind present upstream (Russell and Mulligan, 2002). Classical ICMEs generally present two sub structures. The first one is a compressed

plasma region, usually named sheath, that forms between the shock and the magnetized plasma expelled by the Sun. This structure is characterized by large fluctuations in the magnetic field strength and direction, higher plasma density and temperature than in the upstream solar wind (Kilpua, Koskinen and Pulkkinen, 2017). The following structure, consisting of the plasma expelled by the Sun, has been assigned various names in past studies. In this paper we adopt the magnetic ejecta term. When the magnetic ejecta presents a strong magnetic field and a coherent rotation of its components, along with a low proton temperature and a low plasma beta, this structure is called magnetic cloud (MC, Burlaga, Sittler, Mariani and Schwenn, 1981; Klein and Burlaga, 1982; Dasso, Mandrini, Démoulin, Luoni and Gulisano, 2005).

The other interplanetary structures that usually tend to produce short term decrease of GCRs are SIRs. Several authors have analyzed FDs related with SIRs, analyzing the possible physical mechanisms at the origin of these modulations (e.g., Dumbović, Vršnak, Čalogović and Karlica, 2011; Badruddin and Kumar, 2016; Richardson, 2018; Melkumyan, Belov, Abunina, Abunin, Eroshenko, Yanke and Oleneva, 2019, and references therein). SIRs arise when a fast solar wind flow catches and interacts with slow solar wind flow. The interaction of the two winds form a stream interface where the plasma and the magnetic field are compressed while the flows on both sides are deflected in opposite directions (e.g., Richardson, 2018, and references therein). The fast solar wind typically originates from solar coronal holes (e.g., Krieger, Timothy and Roelof, 1973), while slow solar wind possibly originates from the vicinity of coronal regions with closed magnetic loops (e.g.,

 cgutierrez@iafe.uba.ar (C. Gutierrez)
ORCID(s): 0000-0001-5876-508X (C. Gutierrez)

Gosling, Borrini, Asbridge, Bame, Feldman and Hansen, 1981). When the coronal hole remains during several solar rotation, the associated recurrent SIRs are called Corotation Interaction Regions (CIRs, Richardson, 2018)

As they travel through the heliosphere, both ICMEs and SIRs have an impact on the GCR flux. In particular, when one of these interplanetary structures pass by the Earth, generally, short-term decreases in the GCR flux are observed by detectors located on or nearby Earth. These decreases in the GCR flux were first observed by Forbush (1937) and by Hess and Demmelair (1937), and nowadays they are known as Forbush Decreases (FDs). FDs have been extensively studied by several authors (e.g. Lockwood, 1971; Badruddin, Yadav and Yadav, 1986; Badruddin, Venkatesan and Zhu, 1991; Badruddin, 1996; Simpson, 1998; Melkumyan et al., 2019, and references therein).

Typically the passage of the ICMEs and SIRs near Earth produce different responses on GCRs (e.g., Melkumyan et al., 2019; Dumbović, Vršnak, Temmer, Heber and Kühl, 2022). In particular, from two case study analysis, Raghav, Shaikh, Misal, Rajan, Mishra, Kasthurirangan, Bhaskar, Bijewar, Johri and Vichare (2020) compared ICMEs/SIRs as sources of FDs, using a diffusion/convection model. From a statistical analysis, Melkumyan et al. (2019) found that ICMEs and SIRs have different GCRs modulation abilities. This finding adds an extra interest to deeper understand the differences of FDs produced by these two kinds of solar wind perturbations.

When ICMEs pass near the Earth's surroundings we can usually detect an asymmetrical decrease in the density of GCRs. The observed temporal profile depends on the features of the ICME. A classical ICME tends to produce a two-step FDs (Cane, 2000). The first decrease starts at the shock and continues in the sheath, while the second decrease starts typically at the sheath end and continues within the following magnetic ejecta. The first one has typically a more important amplitude decrease than the second one. The deepest GCR depression is typically in the magnetic ejecta (as it cumulates both previous decreases). Still, there are large event-to-event variations and cases which do not fit this picture. From combining different NMs at different locations, Belov, Abunin, Abunina, Eroshenko, Oleneva, Yanke, Papaioannou and Mavromichalaki (2015) analyzed the effects of ICMEs on the time profile of the GCRs flux outside the Earth magnetosphere. They find that when ICMEs have a flux rope inside, the FD profile is a parabolic function of the distance to the center of the flux rope.

Melkumyan, Belov, Shlyk, Abunina, Abunin, Oleneva and Yanke (2023) statistically compare the FDs profiles produced by ICMEs and SIRs. They started from a catalogue of FDs (taken from IZMIRAN) and then classify them, depending if they are associated with ARs (ICMEs) or CHs (SIRs), emphasizing the solar cycle dependence.

In present paper we continue to analyze the mean properties of both ICMEs and SIRs and their effects on the shielding of GCRs. We study the interplanetary magnetic field and plasma solar wind at the lagrangian point L1,

near the Earth, and the GCR flux measured at ground level by Neutron Monitors (NMs, Simpson, 2000). In particular we analyze data obtained by the MCMurdo NM. We apply the superposed epoch analysis (SEA) technique to find the common features and differences between the FD associated respectively to ICMEs and SIRs.

The SEA is a commonly used method in the area of Space Weather, and particularly in the study of these interplanetary structures (Chree, 1913). In Lepping, Berdichevsky, Szabo, Arqueros and Lazarus (2003), the authors use this approach on a subset of 19 MCs to analyze their common properties. Masías-Meza, Dasso, Démoulin, Rodriguez and Janvier (2016) apply the SEA method to different subset of MCs according to their mean velocity. Other studies apply this technique to study the twisted magnetic field lines in the flux ropes of MCs (Lanabere, Dasso, Démoulin, Janvier, Rodriguez and Masías-Meza, 2020; Lanabere, Démoulin and Dasso, 2022) or the properties of ICMEs (Rodriguez, Masías-Meza, Dasso, Démoulin, Zhukov, Gulisano, Mierla, Kilpua, West, Lacatus, Paraschiv and Janvier, 2016). This last study is extended to a sample of more than 400 ICMEs by Regnault, Janvier, Démoulin, Auchère, Strugarek, Dasso and Noûs (2020). In Janvier, Démoulin, Guo, Dasso, Regnault, Tpsi-Moutesidou, Gutierrez and Perri (2021) the SEA method is utilized several times to analyze ICMEs with and without interplanetary shocks. In Dumbović et al. (2022) the authors apply a SEA to recurrent CIRs associated to a unique coronal hole.

The SEA method was also used to study the variability of GCRs in comparison with geomagnetic storms and interplanetary magnetic field conditions (Kharayat, Prasad, Mathpal, Garia and Bhatt, 2016). In Badruddin and Kumar (2016), the authors do a similar SEA analysis, in which they compare the difference and similarities of FDs caused by ICMEs and SIRs. However, they apply the SEA method differently that we do in this paper. Indeed, in Badruddin and Kumar (2016), the authors take the zero epoch at the arrival time of the ICMEs/SIRs and perform directly the SEA. In contrast we define both arrival and end times for both structures, and we use both times to perform the SEA (so we normalize the time duration, as further explained in Section 4).

In section 2 we present the ICMEs and SIRs we analyze, the catalogues, the data, and the methodology. In section 3 we show two typical events, one ICME and one SIR, and we describe both the generic properties and the peculiarities of each event. In section 4 we introduce and explain the SEA, the reasons to use it, and how we apply the SEA to samples of ICMEs and SIRs. In section 5 we describe the results of the SEA method. We analyze the common and different features of ICMEs and SIRs. First, we apply a SEA to all the sample of ICMEs and SIRs to compare them. Then, we define and apply the SEA to sub samples discriminating by their mean plasma velocity. Finally, we compare ICMEs and SIRs with similar mean velocities. In section 6 we present a summary of our results and our conclusions.

2. Data, catalogues and methodology

Our main aim in this study is to find out the variability differences of the GCR fluxes, when ICMEs or SIRs are the cause of the observed FDs. Thus, we start from catalogues of ICMEs and SIRs, and then we analyze FDs with NM observations for the dates selected in the ICMEs/SIRs catalogues.

In order to analyze the interplanetary magnetic field and the solar wind plasma parameters we use data from the MAG (Smith, L'Heureux, Ness, Acuña, Burlaga and Scheifele, 1998) and SWEPAM (McComas, Bame, Barker, Feldman, Phillips, Riley and Griffee, 1998) instruments aboard the ACE spacecraft. The time resolution of MAG is 16 seconds, and 64 seconds for SWEPAM. ACE was launched on 1997 and since then has provided data almost uninterruptedly. It orbits around the L1 lagrangian point (Stone, Frandsen, Mewaldt, Christian, Margolies, Ormes and Snow, 1998).

To study the flux of GCR we use data from the McMurdo NM with a time cadence of 1 hour (<https://neutronm.bartol.udel.edu/>). NMs are ground based detectors that count neutrons (e.g., Simpson, 2000). These neutrons are generally produced by atmospheric air showers which occur when primary GCRs, that have enough energy, penetrate the Earth magnetic field and reach the low atmosphere. In that situation, these primary GCRs interact with the different atmospheric components and produce secondary particles. Among these particles, one of them are neutrons. Depending on the geographical latitude where the NMs are located, they have a fixed geomagnetic rigidity cutoff. This describes the geomagnetic shielding produced by the Earth's magnetic field against the arrival of the charged primary cosmic ray particles that came from the interplanetary medium. MCMurdo NM station is located in Antarctica and has a rigidity cutoff ~ 0.3 GV.

To study both ICMEs and SIRs we use different catalogues. In order to identify ICMEs events we use the ICME list of (Regnault et al., 2020^[1]), which is a revisited version of the ICME list of Richardson and Cane (2010). We use the Regnault catalogue because it redefines the ICME boundaries, and so, it is more adequate for our analysis. This catalogue gives also information on other features, such as the presence or absence of an interplanetary shock or the presence of MC signatures.

To study the SIRs we use of the Jian, Russell, Luhmann and Skoug (2006) list. This catalogue provides an extensive list of informations per event. In the present work we only use the beginning and ending times of the SIRs. The authors define the SIRs beginning when the total pressure, perpendicular to the magnetic field, starts to increase, and the SIRs ending when the pressure returns to its previous value.

Since we compare below FDs produced by ICMEs and SIRs, we classify both ICMEs and SIRs depending on their mean velocity (computed within the event boundaries). We define three groups with the following criteria:

- i) Slow Event: $-V_x < 450$ km/s
- ii) Medium Event: 450 km/s $< -V_x < 550$ km/s

- iii) Fast Event: $-V_x > 550$ km/s

where V_x is the velocity component in the GSE frame (x axis is directed towards the Sun). This is the same classification as in Masías-Meza et al. (2016) where they found that the bulk velocity of MCs plays a crucial role in the modulation of GCR flux measured at Earth. Compared to this previous work we extend the ICME list, and we perform the same type of analysis on SIRs.

We split the time window of each event, so as to have three equal intervals of time. The first one corresponds to the period of time before the event (pre-event), the next one includes the whole duration of the event taken from the catalogue, and the last one is the period of time after the event (post-event). Before the event, we simply took an interval of time equal to the event duration (to measure the GCR flux before the event in the preceding slow solar wind) and an equal interval of time after the event (to measure the GCR recovery).

Inside ICMEs we distinguish two sub-structures. The first sub-structure goes from the arrival of the interplanetary shock and the beginning of the magnetic ejecta. This region is known as the sheath. It is formed by compressed solar wind plasma with enhanced density, field intensity and temperature. The following sub-structure is known as the magnetic ejecta and includes the plasma expelled during associated coronal mass ejection.

To quantify the modulation in the GCR flux we define the GCR relative counts as:

$$GCR[\%] = \frac{GCR(t) - \overline{GCR}}{\overline{GCR}} * 100 \quad (1)$$

where \overline{GCR} is the mean value of GCR calculated in the pre-event time interval, and $GCR(t)$ is the observed GCR flux at a given time t . The same definition was used in Gutierrez and Dasso (2021), and previous studies (see references in Section 1).

As the main aim of this study is to analyze FDs, we do not consider events where significant ground level enhancements were observed. They consist of an increase in the GCR flux due to a solar event, so they involve another physics than a FD. Our criterion is to remove significant ground level enhancement periods, considering them as cases when the GCR flux reach values greater than 5% above the background GCR (see Equation (1)).

We analyze ICMEs which occurred in the period 1997-2017. This period corresponds to the whole 23 solar cycle and most of the 24 solar cycle. The ICMEs catalogue has data of ICMEs since 1995. However, SWEPAM started to measure at late 1997, that is why we only study events from 1997, and we studied ICMEs till 2017 corresponding to the year when McMurdo NM has ceased its operations. We only study ICMEs with sheaths, because one of the objectives is to observe the different behaviour of the ICME sub-structures.

We study all SIRs that occurred in the period 1997-2009. The reason is the same as for ICMEs, the instruments of

¹https://idoc.ias.u-psud.fr/sites/idoc/files/CME_catalog/html

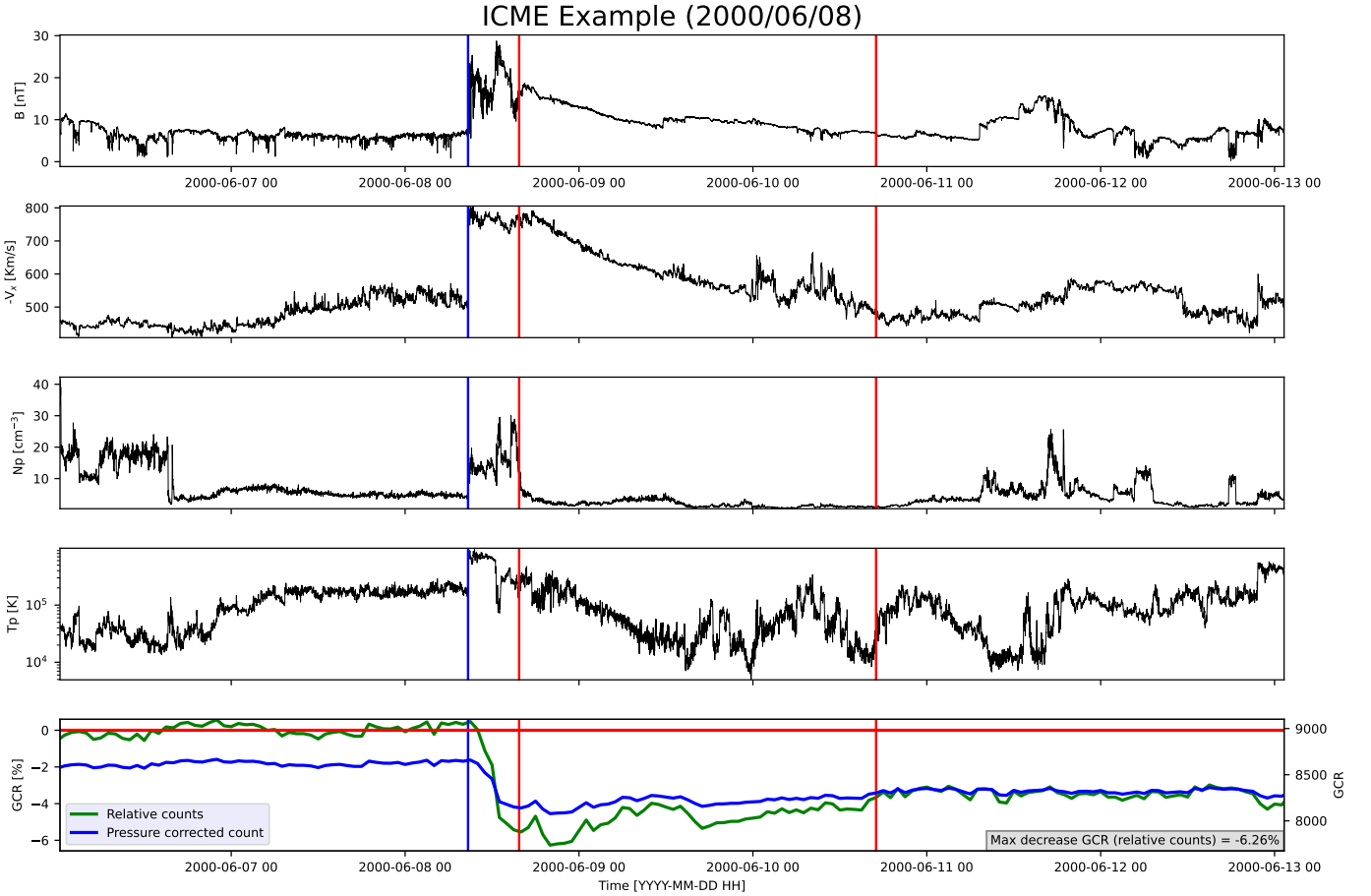


Figure 1: An ICME observed on 8th June 2000 by the ACE spacecraft. The first (top) panel corresponds to the interplanetary magnetic field B . The second panel shows the solar wind speed $-V_x$ (GSE component) so that $-V_x$ is directed away from the Sun. The third panel corresponds to the proton density N_p . The fourth panel shows the proton temperature T_p . Finally, the fifth panel shows the neutron counting rate per hour (proxy of the galactic cosmic ray flux) measured by the McMurdo NM (the scale is on the right side). The blue line corresponds to the pressure corrected counts (scale on the left side), while the green line corresponds to the relative counts, which is calculated with Equation (1). The solid horizontal red line represents the reference level (based on the mean value before the ICME) for the relative counts. The blue vertical lines in all the panels represent the arrival of the interplanetary shock, whereas the red solid vertical lines represent the beginning and ending of the magnetic ejecta. The ICME sheath is present behind the shock (before the first red line). It is formed by solar wind plasma and magnetic field accreted in front of the magnetic ejecta.

ACE started their operations in 1997 and the SIR catalogue ends in 2009. This period corresponds to the whole 23 solar cycle. During the solar cycle maximum ICMEs are more numerous due to the higher solar activity, while during the solar minimum SIRs dominate.

3. Two typical events

In this section we present two events, as examples of typical cases. One event corresponds to an individual ICME and the other one corresponds to a SIR. We analyze the events and explain the reasons why we consider that applying a SEA provides robust results for the FDs produced by both structures.

3.1. ICME on 8 August 2000

In Figure 1 we show an example of an ICME. The first panel from the top shows the absolute value of the interplanetary magnetic field. In the second panel, we show the x GSE component of the solar wind speed. The third panel corresponds to the proton density. The fourth panel shows the proton temperature. The final panel shows the GCR flux, the blue line represents the pressure corrected NM count rate (per hour) and the green line the relative counts calculated with Equation (1). The inset, at the bottom right, provides the value of the minimum GCR flux inside the time window of the ICME. The blue vertical line in each panel represent the interplanetary shock arrival time, the red vertical solid lines represent the magnetic ejecta start and end, respectively.

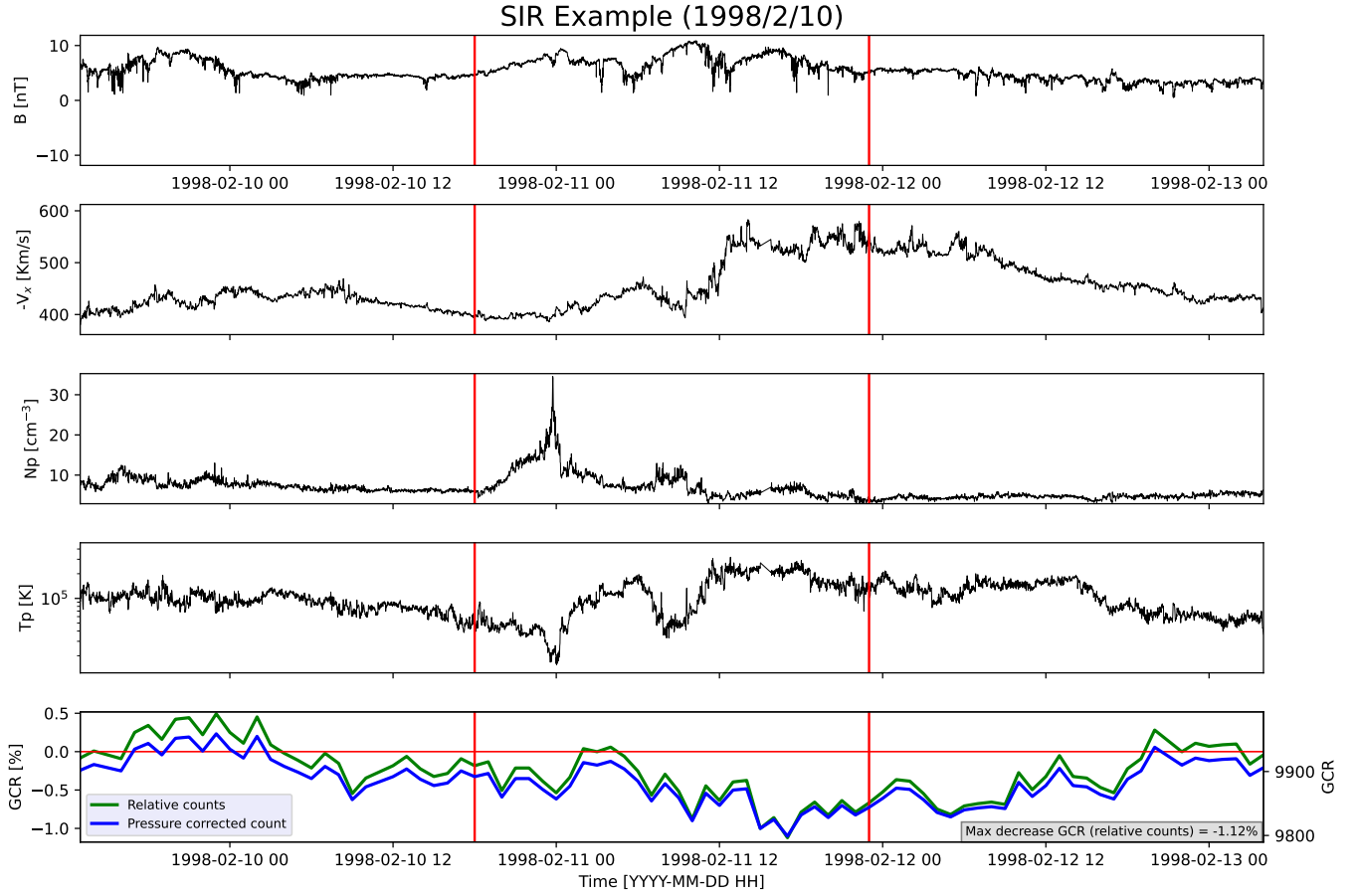


Figure 2: A SIR observed on the 10th February 1999 by the ACE spacecraft. The panels and the format are the same as Figure 1, with the only difference in the vertical lines, which in this case only represent the beginning and the end of the SIR respectively (a shock is not present).

In Figure 1, a fast solar wind is present before the arrival of the interplanetary shock with a mean velocity of ~ 500 km/s. At the time of the interplanetary shock arrival the typical jumps for B and plasma parameters are present. The jump of $-V_x$ is the most remarkable with a sudden increase from ~ 500 km/s to ~ 800 km/s. Then, it is a fast ICME according to our classification. During the sheath crossing, there is a $\sim 5\%$ decrease in the GCR flux at McMurdo. After the magnetic ejecta starts, an almost monotonous decrease of B is present. Next, $-V_x$ has a decreasing profile associated with the ICME expansion as it propagates in the interplanetary medium. A second weaker decrease of GCR flux is caused by the magnetic ejecta. This decrease is of $\sim 1\%$, five times weaker than the decrease observed during the ICME sheath. Once the ICME ends, the interplanetary magnetic field and the plasma parameters start to return to the values present before the ICME (i.e., the pre shock solar wind). However, the GCR flux remain $\sim 4\%$ weaker with respect to its value before the ICME.

One of the benefits of applying a SEA is that the fluctuations in the profiles of all parameters are removed in the mean profiles of ICMEs (see Section 5.2).

3.2. SIR on 13 January 1999

In Figure 2 we show an example of a SIR. The figure has the same format as Figure 1, with the exception of the absence of a shock. The two red vertical solid lines represent the start and end of the SIR according to the Jian et al. (2006) list. One may argue that the end boundary is earlier, at about 19 UT on 11 February, where $-V_x$ has a local increase while other quantities (B , N_p , T_p) decrease. Such ambiguity of boundaries is also present in a small fraction of SIRs. However, shifting the boundaries of such events has only a small effect on the SEA results (as shown by Regnauld et al., 2020, for ICMEs). Then, there is no point to argue in favor of any of these ambiguous boundaries in this paper.

The measured velocity shows a clear slow solar wind regime before the SIR with $-V_x \sim 400$ km/s, then an increase at the stream interface to $-V_x \sim 550$ km/s. This increase is accompanied by an increase of T_p , which is expected in fast wind since there is a correlation between T_p and $-V_x$ in the solar wind (e.g. Lopez and Freeman, 1986; Démoulin, 2009). Since SIRs include compressed slow solar wind interacting with fast solar wind, some adiabatic heating of the SIR plasma is expected (Elliott, Henney, McComas, Smith and Vasquez, 2012). Indeed, a slightly higher T_p is present

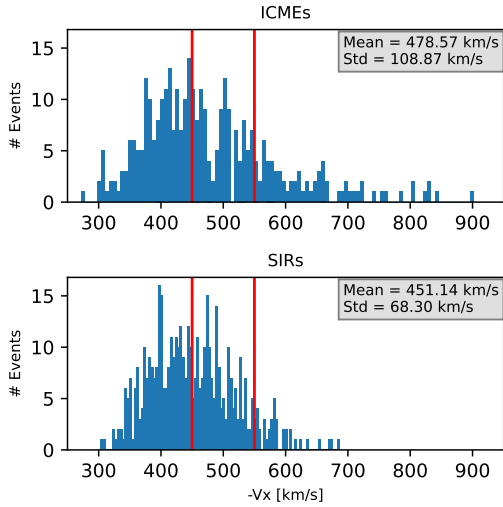


Figure 3: (top) histogram of mean $-V_x$ for ICMEs. (bottom) histogram of mean $-V_x$ for SIRs. The vertical red lines represent the borders for slow, medium and fast events.

after the stream interface compare to T_p measured after the SIR within a wind of similar $-V_x$ value. Next, the GCR flux decreases during the passage of the SIR near Earth, reaching a minimum value of $\sim 1\%$. However, this decrease is smaller than that during the ICME shown in Figure 1, even when local in-situ values of B and $-V_x$ have similar values. Also the shape of the profiles are different: in the case of SIRs the decrease is somewhat linear, reaching the minimum of GCR flux at the end time of the SIR, whereas in the ICME the GCR flux minimum is reached near the beginning of the ejecta.

Above, we describe the main features of the SIR shown in Figure 2. However, this SIR, as most other SIRs, has also peculiarities specific to each event. For example, there are a prominent density spike at the end of February 10 and an unusual region of reduced temperature before the mid February 11. Some local modulation of the observed GCR flux could be due to these local peculiarities. The strength of the SEA is to minimize these local peculiarities, which are associated to only one or a few events, and to emphasise the common properties of SIRs.

4. Superposed epoch analysis

Each ICME event has its own peculiarity and fluctuations, then to find the typical features of ICMEs, and to remove these peculiarities, one of the best technique to apply is a SEA, also known as Chree analysis (Chree, 1913).

The SEA is a statistical method which consists in obtaining mean profiles from a sample of individual profiles. In order to be superposed, each individual event must have the same number of data points in the time dimension to obtain the average values of the physical parameter considered. In our case, each event has different duration, and so, a different

number of data points. To get rid of this we rebin so that each event have the same number of data points.

The binning is slightly different for each type of event. For SIRs we decided to take 100 time bins before the SIR, 100 time bins inside the SIR and 100 time bins after the SIR, for both magnetic and plasma data. Due to the fact that ICMEs present two sub-structures (sheath and magnetic ejecta), we divide the event window in two. In general magnetic ejecta have longer duration than sheaths. That is why we define more time bins for the magnetic ejecta than for the sheath. Following the statistical results of Regnault et al. (2020), we take 100 time bins before the ICME, 100 time bins inside the ICME (30 for the sheath and 70 for the magnetic ejecta) and 100 time bins after the ICME. In both cases we assign the mean value inside each time bin interval to the corresponding bin.

The time axis is normalized with an origin set at the beginning of the ICME/SIR and the end of the ICME/SIR is set to 1. This implies that -1 and 2 corresponds respectively to the normalized time at the beginning and the end of the data considered.

In case of GCR data we take only 30 time bins per event because we have lower temporal resolution and more fluctuations. This lower resolution, by a factor 10 compared to above, allows to decrease the fluctuation level of the GCRs, and leads to a clearer signal. In case of SIRs we take 10 time bins before the SIR, 10 time bins inside the SIR, and 10 time bins after the SIR, for GCR data. In the case of ICMEs we take 7 time bins before the ICME, 13 time bins inside the ICME (6 for the sheath and 7 for the magnetic ejecta), and 10 time bins after the ICME, for GCR data. Finally, for each physical parameter, we assign the mean value inside each time bin interval to the corresponding bin.

One of the main limitation that arises from applying a SEA is that the amplitude of the FDs (i.e. the minimum of the GCR flux) obtained in the SEAs results in an underestimation of the real value. The reason is that in general each individual event can have its minimum GCR flux at a different time bin. It implies that SEA provides a smoothed profile, with a weaker minimum than the mean value of the minimum of events.

5. Results

In this section we present the analysis of the sample of events we study. We analyze 344 ICMEs in the period (1997-2017) and 450 SIRs in the period (1997-2009). We have 177 slow, 98 medium, and 69 fast ICMEs, compared to 239 slow, 172 medium, and 39 fast SIRs according with our classification (Section 2).

In Figure 3 we show the histograms of the mean value of $-V_x$ within ICMEs and SIRs. They both have very similar global mean speed (479 km/s for ICMEs and 451 km/s for SIRs). The standard deviation is 109 km/s for ICMEs and 68 km/s for SIRs. Indeed, the distribution of $-V_x$ for ICMEs is wider, since it has a longer tail toward faster events than the distribution for SIRs. Apart this tail difference, involving a minority of cases, ICMEs and SIRs have comparable mean

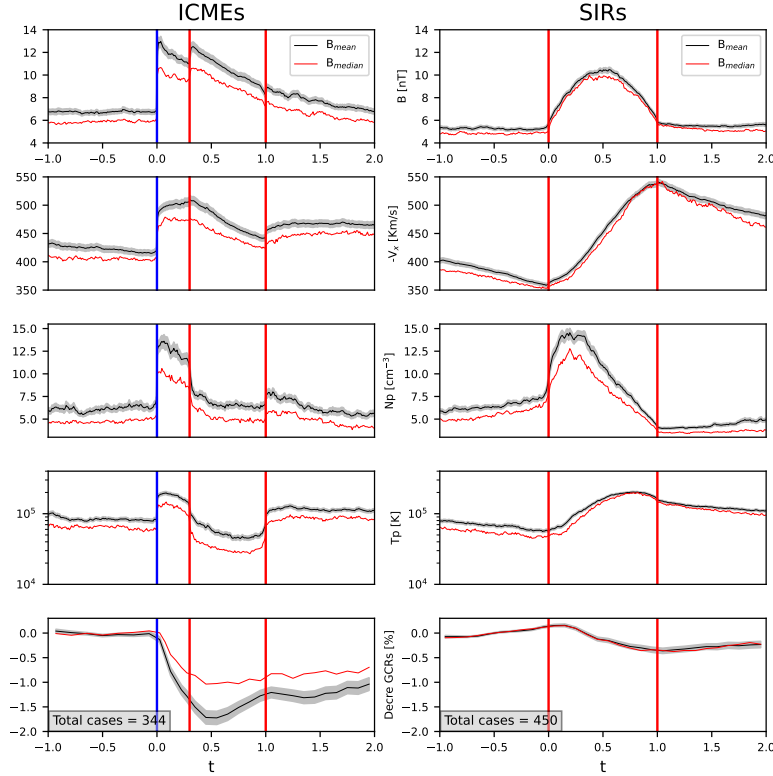


Figure 4: Comparison between the SEA applied to all ICMEs and all SIRs. The five panels represent the same parameters studied in Figures 1 and 2. The left panels correspond to ICMEs. The three time windows have the same normalized time. -1 is the beginning of the time window considered, 0 is the ICME start (arrival of the interplanetary shock), 1 the ICME end, and 2 is at the end of the time window considered. The intermediate red vertical line represent the beginning of the magnetic ejecta. The bottom panel shows the number of cases considered for the superposed epoch analysis. The black lines represent the SEA taking the mean values and the red lines the SEA considering the median values. The grey shaded region is the error region. The right panels correspond to the SIRs. All the drawing conventions are the same with the only difference being the vertical lines. In this case the red lines represent the SIR front and end.

velocity distributions. In the next sub-sections we focus our analysis on the differences between the typical profile of FDs produced by ICMEs/SIRs.

5.1. Comparison between ICMEs and SIRs

First we compare the SEA profiles of all ICMEs with respect to the SEA profiles of all SIRs (Figure 4). This allows us to investigate the typical differences between ICME and SIR profiles. The order of the parameters plotted is the same as in Figures 1 and 2.

The typical B profile of SIRs has a parabolic shape profile, with its maximum at the middle of the structure. In contrast, in ICMEs a great discontinuity is present at the beginning (shock), followed by an almost linear monotonous decrease. The B strength present before the events is less in SIRs (~ 5 nT) than in ICMEs (~ 7 nT). At the end of the SIRs, B recovers immediately its before event value, while in ICMEs, B continue its decrease, with the same slope, once the ICMEs have passed.

The leading parts of the profiles in Figure 4 are similar to the ones presented in a SEA study that focussed on a comparison of the impact of ICMEs/SIRs on geomagnetic

perturbations (Badruddin and Falak, 2016). In particular, their Figure 1 shows a larger B for ICMEs than for SIRs, and also a more symmetric B profile for SIRs. However, since these authors fixed only the starting point of ICMEs/SIRs and they kept the physical time without normalization for their SEAs, the full shapes are not comparable to the one we obtain here.

The $-V_x$ profiles are also clearly different. In SIRs, $-V_x$ increases during all the event. This is a consequence of the stream interaction, as the fast solar wind flow catches the slower solar wind flow ahead of it. Again, the shape of this profile around the starting point of the SIR is similar to the one obtained by Badruddin and Falak (2016). In contrast, the $-V_x$ profile of ICMEs has a jump of $-V_x$ at the arrival of the interplanetary shock, then a slight increase in the sheath, and a continuous decrease that is associated to the global ICME expansion as they propagate in the interplanetary medium (e.g., Démoulin and Dasso, 2009). Here our results differ with those of Badruddin and Falak (2016) since they did not split the ICME into the two sub-structures sheath-ejecta.

The density profile in SIRs is characterized by an initial increase which could be due to the heliospheric plasma sheet

ahead of, or being swept into the SIR. Later on a nearly linear decrease, down to the value of the fast catching solar wind, is present. This behavior may be the result of the stream interface being smeared out by the choice of zero epoch at the SIR leading edge (rather than on the stream interface), so that we can compare SIR and ICME profiles. A similar behaviour is observed within ICMEs, first an increase associated with the arrival of the interplanetary shock, then of the sheath. It is followed by a density decrease since the magnetic ejecta is typically under dense. However, the ICME/SIR profiles have also some differences due to the different physics involved. For a SIR a typically dense slow solar wind is catch up by an under dense fast wind. For the sheath, the plasma is first compressed by the shock, then by the catching up ejecta. Then, the plasma is under-dense because the ICME expands as it propagates away to the Sun.

The proton temperature, T_p , increases in SIRs because the fast wind is typically hotter than the slow one (Lopez and Freeman, 1986) and plausibly, at least, by adiabatic heating as the plasma is compressed (Elliott et al., 2012), while in the magnetic ejecta, T_p decreases by adiabatic cooling during the expansion (there is still some heating otherwise magnetic ejecta would be cooler than observed at 1 au).

Finally, the modulation in the GCR flux during SIRs or ICMEs is noticeable different. In ICMEs the decrease is deeper, with a minimum value of $\sim 1.25\%$ (for the mean value), a factor 5 larger than in SIRs. Another difference is the shape of the decrease. In SIRs, a gradual decrease starts a little after the SIR start (when N_p reaches its maximum value). In ICMEs, on the other hand, the decrease begins immediately after the interplanetary shock arrival and continue within the sheath, then within the front part of the magnetic ejecta.

Another difference is the location of the minimum GCR flux. The GCR flux minimum is at the end of SIRs. This is in agreement with Badruddin and Kumar (2016) while they were using Oulu and Newark NM data (with higher cut-offs than McMurdo used here) and they were also using a SEA with a different zero epoch setting. We conclude that the location of the GCR flux minimum in SIRs is robust. In contrast to SIRs, the GCR flux minimum is at the middle of ICMEs. It is worth to recall that there is a temporal dispersion of GCR minimum in individual events so the SEA introduces a smearing effect. Still, the SEA reveals a well marked global difference between ICME and SIR profiles of GCRs.

We end up by comparing our SEA results to the data of individual events shown in Figures 1 and 2. To shorten the text, we compare below only the GCR flux of the SIR case, while the same can be easily adapted to other parameters and the ICME case. Indeed, when we apply the SEA to SIRs we find that the GCR flux is strongly smoothed with respect to an individual SIR. What is specific to the SIR shown in Figure 2 could be found by comparing the observed profiles to those obtained with the SEA of SIRs (Figure 4). In particular, in Figure 2, the GCR flux has an extended period (about 15 h) of lower flux before the SIR, then a series of

minima are present within the SIR as well as an enhanced GCR flux at the beginning of 11 February. Since these local features do not appear in the SEA of SIRs, they are not shared by many events. More details of this SIR were described at the end of Section 3.2. Furthermore, SEA allows the weaker, though common, features to be discerned while they may be dominated by local peculiarities in individual events. For example, the parabolic shape of B is well present in the SEA of SIRs, while B in the individual SIR is much noisier, as in Figure 2.

5.2. ICME SEA

Some previous studies have statistically analyzed the dependence of the amplitude of Forbush decreases with the intensity of the magnetic field and/or the bulk velocity inside the solar wind structures that produce them (e.g., Melkumyan et al., 2019; Badruddin et al., 1986). Dumbović, Vršnak, Guo, Heber, Dissauer, Carcaboso, Temmer, Veronig, Podladchikova, Möstl, Amerstorfer and Kirin (2020) developed a model (ForbMod) to explain why faster ICMEs show larger FD amplitude than slow ones. They concluded that faster ICMEs had less time to fill in with GCRs than slow ones, via cross-diffusion. This model includes a filling factor related with the ICME age (i.e., slow ICMEs have more time to fill their interior via cross-diffusion during their Sun-Earth travel).

In Figure 5 we show the results of applying the SEA technique to slow, medium and fast ICMEs. This figure is very similar to the Figures 4 and 6 of Masías-Meza et al. (2016). However, these authors apply the SEA to a subset of 44 MCs. In this study we apply the SEA to 344 ICMEs, without distinction of MC features. Analyzing B before the ICME arrival (before the shock), we observe $B \sim 5$ nT for slow ICMEs, $B \sim 8$ nT for medium and fast ICMEs. This is consistent with the results reported by Masías-Meza et al. (2016) for the case of MCs, and consistent with finding slow ICMEs travelling in a magnetically weaker pre solar wind. At the interplanetary shock arrival, we observe the jump in B . B goes from from ~ 5 nT to ~ 11 nT in slow ICMEs, while in fast ICMEs B goes from ~ 8 nT to ~ 20 nT. Inside the sheath of medium and fast ICMEs an asymmetric B shape is present, with its maximum B at the leading edge. This behaviour is not so clear in slow ICMEs.

Regarding $-V_x$ before the ICME arrival, we observe slow solar wind of ~ 400 km/s in slow ICMEs, ~ 420 km/s in medium ICMEs, and fast solar wind speed regime of ~ 500 km/s in front of fast ICMEs. This result is also in agreement with Masías-Meza et al. (2016), and consistent with a slow down mechanism (e.g., via drag) for ICMEs travelling in slow solar wind. More precisely, the difference of velocity between the ICME and the encountered wind is larger as the wind is slower, more over the density is larger, so the drag is more efficient in a slower wind. This implies that slower ICMEs at 1 au are more frequently travelling in a slower solar wind.

Slow ICMEs sheaths expand, whereas fast ICMEs sheaths are in compression. This phenomena was also observed and

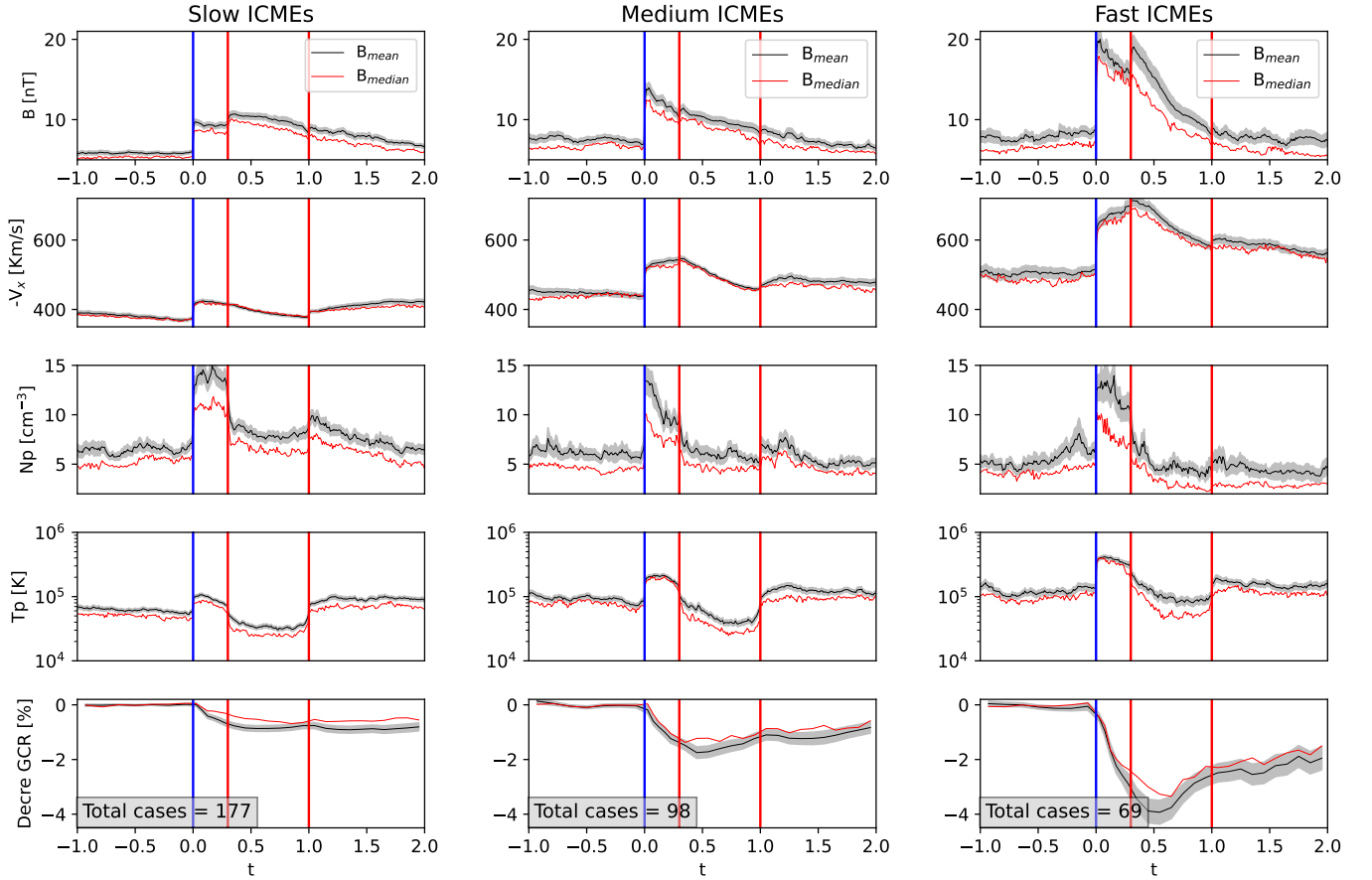


Figure 5: Superposed Epoch Analysis for the slow ICMEs (left), medium ICMEs (middle), and fast ICMEs (right). The five panels represent the same parameters studied in Figure 1. The three time windows have the same normalized time. -1 is the beginning of the time window considered, 0 is the ICME start, 1 the ICME end, and 2 is at the end of the time window considered. The bottom panels show the number of cases considered for each superposed epoch analysis. The black lines represent the SEA taking the mean values and the red lines the SEA considering the median values. The grey shaded region is the error region. The blue vertical line represents the interplanetary shock, the two red vertical lines represent the beginning and ending of the magnetic ejecta.

explained in Masías-Meza et al. (2016) and Regnault et al. (2020). Sheaths are compressed in fast ICMEs due to the interaction of the following fast magnetic ejecta, while for slow ICMEs the magnetic field and plasma have the time to reach a quasi-pressure balance. This implies an expansion similar to that of a flux rope (as modeled by Démoulin and Dasso, 2009). Next, inside the magnetic ejecta a clear expansion is present for all ICME groups as found previously in other works (e.g. Rodríguez et al., 2016).

The proton density N_p shows its higher value inside sheaths. This maximum in N_p is associated with the compression that takes place when the pre-shocked plasma passes through the interplanetary shock. A peak of N_p is present just behind the ICME end for the three ICME classes. The plausible origins of this peak is explained in detail, for the case of MCs, in Rodríguez et al. (2016). In the majority of events this density peak could be associated to the compression by a trailing fast-stream. A strong internal expansion of the magnetic ejecta could also explain this

density peak for a small fraction of events. Finally, a third plausible origin could be present at the solar origin (e.g. the compression by a reconnecting jet behind the erupting flux rope).

After the interplanetary shock arrival, inside the sheath, an increase in T_p , associated with the heating, takes place. During the magnetic ejecta we see a T_p profile associated with a cooling, due to a combination between expansion and cooler initial coronal conditions (Démoulin, 2009). The temperature contrast is similar in all ICME classes, implying that T_p is globally higher in faster ICMEs.

Finally, we analyze the GCR flux response. At the beginning of all ICMEs, a decrease in the GCR flux is observed. This decrease is more noticeable in faster ICMEs than in slower ones, consistently with a well known result (see, e.g., Regnault et al., 2020; Janvier et al., 2021). In slow ICMEs, the observed decrease is small with a relative minimum of $\sim 1\%$, in medium ICMEs the minimum is of $\sim 2\%$ and the biggest decrease is observed in fast ICMEs with $\sim 4\%$.

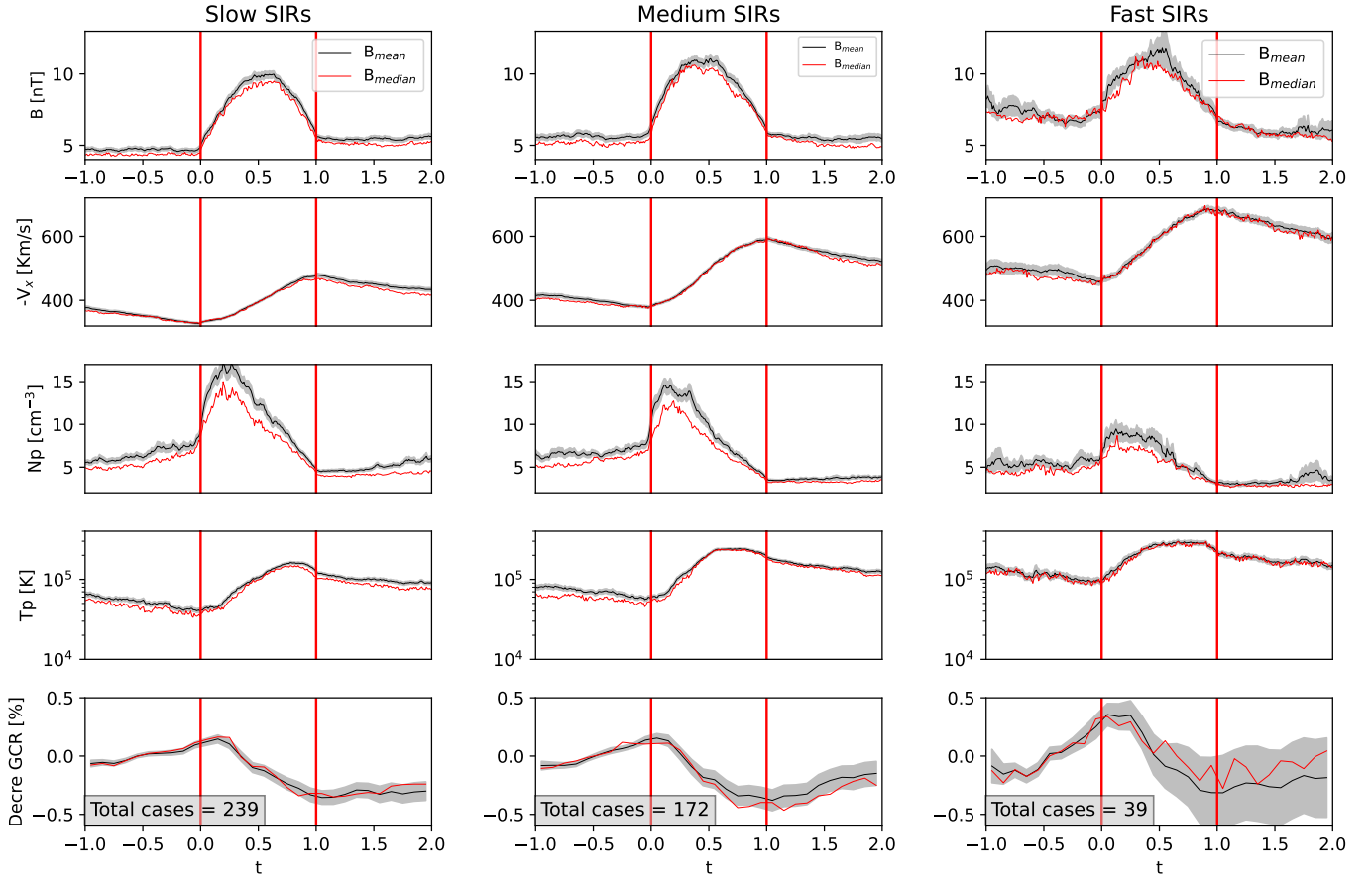


Figure 6: Superposed Epoch Analysis for the slow SIRs (left), medium SIRs (middle), and fast SIRs (right). The five panels represent the same parameters studied in Figure 2. The three time windows have the same normalized time. -1 is the beginning of the time window considered, 0 is the SIR start, 1 the SIR end, and 2 is at the end of the time window considered. The bottom panels show the number of cases considered for each superposed epoch analysis. The black lines represent the SEA taking the mean values and the red lines the SEA considering the median values. The grey shaded region is the error region.

Other difference regarding the GCR flux is their profiles. Fast ICMEs are the ones that resemble the most to the classical two step FD associated to ICMEs. We distinguish two different slopes. The first slope is associated with the sheath, and a second one, less steep, is associated with the beginning of the magnetic ejecta. Once the event has passed, the recovery phase is longer than the ICME extension for all cases.

5.3. SIR SEA

In Figure 6 we present the results of applying the SEA method to our sample of events, splitting in slow, medium and fast SIRs. The profiles of all the parameters have a similar behaviour (in contrast to ICMEs). We can not find remarkable differences between slow, medium and fast SIRs, apart a variation of amplitude. Indeed, the B profiles in all SIRs have a parabolic shape with a maximum in the SIR middle of ~ 10 nT, ~ 11 nT and ~ 12 nT for slow, medium and fast SIRs respectively. One of the differences between the profiles resides in the B intensity before the starting time of

the SIRs, being ~ 4 nT, ~ 6 nT, and ~ 8 nT for slow, medium and fast SIRs respectively.

The $-V_x$ profiles have the same behaviours. Once the SIR begins, $-V_x$ starts to increase monotonously until the end of the SIR. Once the SIR ends $-V_x$ starts to decrease. As for B intensity, the upstream speed is faster for faster SIRs. This is the same ordering than for ICMEs. However, for SIRs the main effect may be not physical, as for ICMEs, but due to our definition of the SIR velocity. We define the SIR speed as the mean within the boundaries, so it includes a part of the slow solar wind present in front of the stream interface, so faster SIRs are expected to have a faster upstream (as well as downstream) wind. Then, these faster upstreams have a larger B intensity (as for ICMEs).

The N_p behaviours are also the same for all SIRs. The density increases until a maximum value located near the stream interface, and then, it decreases to its previous value. More surprising the density increase in the SIR is larger for slower SIRs. This is related to a larger increase of B , relative to its value before the SIR front, for slower SIRs. This points to a stronger compression of the slow solar wind in slower

SIRs, which could be related to a longer interaction time of the streams (longer travel time). Finally, the density is lower behind the faster SIRs simply because a faster wind is present and it is typically less dense.

The main temperature increase is a consequence of a faster, so hotter, solar wind behind the SIR. However, there is a larger T_p , than in the following solar wind, in about the second half of the SIRs. Even more, this higher temperature region is more marked and extended for faster SIRs. We interpret it as the consequence of heating, at least by compression as traced by the $-V_x$ profile. The effect of compression is clearer on N_p and dominantly present in the first half of the SIR. This points for the need of extra heating to increase T_p in the second half of the SIR.

All SIRs have very similar GCR flux profiles, with more dispersion for the fast SIRs since they are less numerous (so individual peculiarities are less minimised). A progressive increase of the flux is present well before the SIR and it ends significantly after the SIR start. The decrease of GCR flux begins at the maximum N_p in all SIR groups. Next, there is an anti-correlation between $-V_x$ and GCR flux in the line of previous results (e.g., Badruddin et al., 1986).

Finally, the GCR flux decreases until the end of the SIR. The most remarkable feature is the location of the minimum GCR flux, which is near the end of the SIRs for the three groups. The minimum amplitude of the GCR flux is $\sim 0.35\%$, $\sim 0.38\%$ and $\sim 0.31\%$ for slow, medium and fast SIRs respectively. We can then conclude that the mean solar wind velocity in SIRs is not a good parameter to infer the FD amplitude, in contrast to the results obtained for ICMEs (Figure 5).

5.4. Comparison between ICMEs and SIRs

Now we compare the FDs caused by ICMEs and SIRs with similar velocities. We observe from Figures 5 and 6 that in case of slow events, both ICMEs and SIRs produce weak FDs (in terms of FD amplitude). The minimum GCR flux in slow ICMEs is $\sim 0.85\%$, while in slow SIRs, the FDs amplitude is $\sim 0.35\%$. However, the profile of the decrease is different. For FDs produced by SIRs, the GCR flux is very well anti-correlated with the solar wind speed (in concordance with Richardson, Wibberenz and Cane (1996)); while in the case of FDs driven by ICMEs, the solar wind speed velocity and the GCR flux do not present such anti-correlation.

When we analyze fast events, we observe that the FDs produced by ICMEs and SIRs are clearly different. In fast SIRs, the maximum amplitude of the FDs is $\sim 0.31\%$, while in fast ICMEs, it reaches a value of $\sim 3.92\%$. That is, FDs produced by fast ICMEs are more than 11 times higher than those produced by fast SIRs.

We summarize the main results of the ICME/SIR comparison in Figure 7. We compute the mean value of the bulk velocity, within the events, from the SEA mean for the three groups classified as slow-medium-fast. The error bars correspond to the average of all errors during the ICME/SIR event in each of the SEA. From this, we can observe that

fast ICME/SIR events exhibit more uncertainties than slow ICME/SIR events. This is primarily due to the fewer number of fast ICME/SIR events compared to slow ones. This can also be verified by examining Figures 5 and 6, where the area of uncertainty is larger in fast ICME/SIR events than in slow ones. Taking the median, at the place of the mean, shows very similar results (so they are omitted). The FD amplitude is the maximum decrease of GCR during the SEA of ICME/SIR. The FD amplitude is independent of the mean velocity for SIRs while there is a strong dependence for ICMEs (Figure 7 left panel). These results are consistent with the ones reported by Melkumyan et al. (2019), where other techniques were used. Next, for ICMEs, a strong dependence of FD amplitude is present in function of the maximum magnetic field strength, B_{max} (Figure 7 right panel). In contrast B_{max} has almost the same value in the three SIR groups.

In summary, our conclusion from Figure 7 is that SIRs' FDs do not depend on their mean velocity while it appears to be the case for ICMEs' FDs. However, B_{max} is also a key parameter to determine FD amplitude for ICMEs. Moreover, it is striking that both B_{max} and FD amplitude are similar in the three SIR groups. If we suppose that the GCR screening process is similar in SIRs and ICMEs, this result points to a major screening effect of B_{max} in both type of events. In this case, the relationship of FD amplitude with the mean velocity for ICMEs would only be an indirect consequence of the correlation between the mean velocity and B_{max} .

6. Summary and conclusions

We analyze 457 ICMEs in the period (1997-2017) and 450 SIRs in the period (1997-2009). We study the SEA of ICMEs and SIRs with the same method, rescaling the events in time so that both their leading and following boundaries are superposed. Analyzing the SEA time profiles for FDs driven by ICMEs and SIRs, we noticed different response in the GCR flux. The FD intensity is weaker for FDs produced by SIRs with respect to the FDs produced by ICMEs. Analyzing all the ICMEs and SIRs we find that the maximum depression of the GCR flux is $\sim 1.8\%$ for ICMEs and $\sim 0.35\%$ for SIRs. This result is in concordance with the result of Badruddin and Kumar (2016), where they find that the average maximum depression of GCRs in ICMEs is $\sim 1.5\%$ and $\sim 0.5\%$ for SIRs.

We also notice a previous increase of the GCR flux before the leading edge of SIRs but not for ICMEs. This behaviour is also reported in Dumbović et al. (2022). However, there are some differences in the analysis. In Dumbović et al. (2022), the authors analyze a single coronal hole that produce 27 CIRs, while in this paper we analyze all the SIRs which occurred in 1997-2009. Another differences reside in the definition of the events. We define the SIR boundaries according the Jian et al. (2006) list. In Dumbović et al. (2022), they define the beginning of the SIR with the same criteria while they define the end of the SIR when the solar wind velocity return to the value present before the SIR.

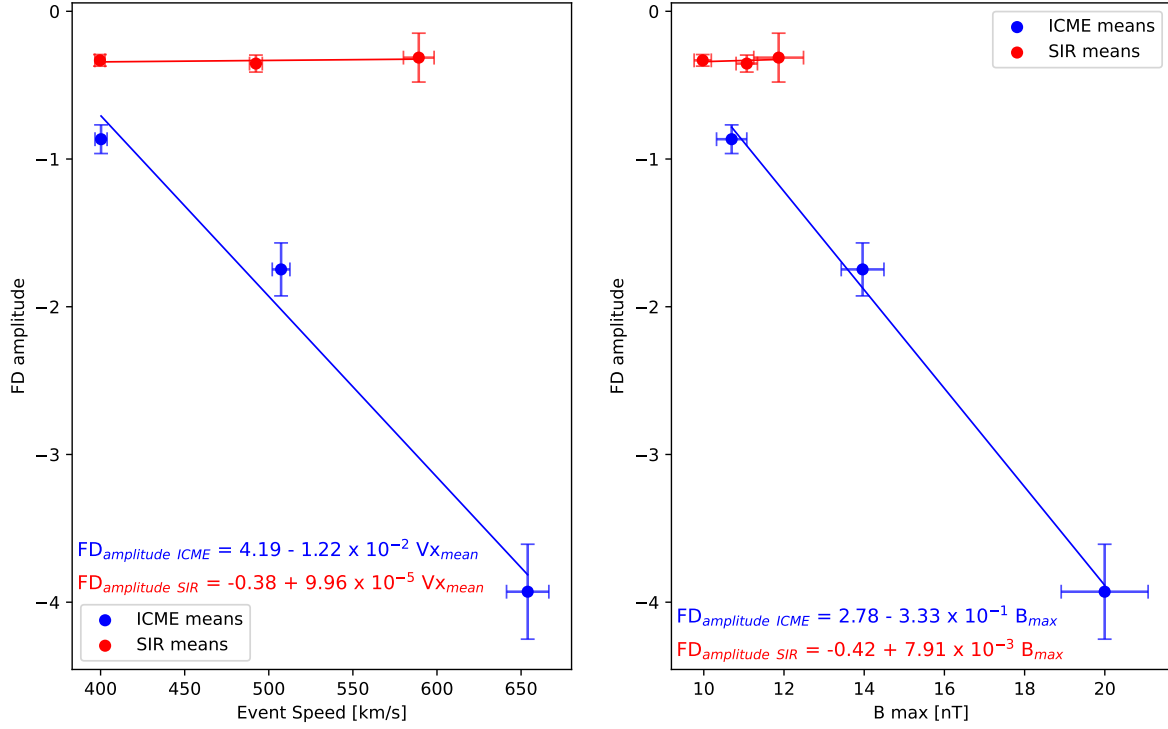


Figure 7: Plots summarizing the results of slow, medium, and fast ICMEs/SIRs shown in Figures 5 and 6. The FD amplitude denotes the maximum decrease of GCR during the ICME/SIR. The FD amplitude is plotted in function of the mean speed (left panel) and the maximum magnetic field strength, B_{max} (right panel), of the SEA. The linear regression lines for ICMEs/SIRs are added. The error bars correspond to the average of all errors during the ICME/SIR event in each of the SEA.

This differs from our case where the SIR is defined as the compression region (as defined by Jian et al., 2006) and it does not include the following fast solar wind stream. This SEA result a posteriori further justify how Jian et al. (2006) defined the end of SIRs.

Another difference between the FDs produced by ICMEs and SIRs is their profile. In ICMEs, a decrease in the GCR flux begins at the arrival of the interplanetary shock and reaches its minimum at almost the middle of the ICME. In other words, the GCR minimum is a little after the beginning of magnetic ejecta. Later on, a monotonic recovery of the GCR flux is present. It extends during a time period longer than the time window considered for the analysis. For the case of SIRs, a decrease of the GCR flux is present during the main part of the SIR where the magnetic field is enhanced and where the radial velocity increases with time (so with an anti-correlation with the solar wind velocity as previously found, e.g. Richardson, 2004). Then, the GCR flux is minimum at the SIR rear.

We also find that the mean solar wind velocity plays a key role in the modulation of GCRs in ICMEs. In slow ICMEs, a weak FDs is observed ($\sim 0.85\%$), while in fast ICMEs the FDs intensity is $\sim 3.92\%$, so more than four times higher. However, in the case of SIRs we observe that FDs are not dependant on the mean bulk solar wind velocity. Slow, medium and fast SIRs have very similar FDs decrease, with values of $\sim 0.35\%$, $\sim 0.38\%$ and $\sim 0.31\%$ respectively. The

shape of the FD, as well the B profile, is also similar in the three SIR categories.

Finally, we find that the FD amplitude produced by SIRs or ICMEs is not so different for slow events, but significantly different for fast ones. For instance for fast SIRs the GCR flux reaches a value of $\sim 0.35\%$, but for fast ICMEs it reaches $\sim 3.92\%$. Then, in spite of having similar velocity, fast ICMEs produced 10 times higher FDs with respect to fast SIRs. In fact the main difference is magnetic field intensity: it increases strongly with faster ICMEs, so does the FD amplitude. In contrast, for SIRs both magnetic field intensity and FD amplitude are nearly independent of the mean speed. This points for the magnetic field intensity to be the main screening agent of GCRs in ICMEs and SIRs.

Results presented here will help to better understand the physical mechanisms for the transport of energetic particles (e.g., protons of $\sim 1-10$ GeV) in different transient plasma regimes of the solar wind. Above results set observational constraints to models and simulations of GCRs since they need to reproduce/explain them within the same framework, taking into account the different geometries and magnetic configurations of ICMEs and SIRs. For example, the generic presence of an increase of GCR flux before SIRs and not before ICMEs is challenging. Another point is to clarify the weaker role of plasma velocity than the one of magnetic field as the contrasting results of ICMEs/SIRs show.

There are also other aspects to consider, such as the topology of the magnetic field. In the case of ICMEs, where the presence of flux ropes or closed magnetic field structures dominates, the response in cosmic ray flux is different than in the case of SIRs, which are characterized by open magnetic field structures. We expect that more results will come in the next years, for instance from new generation of ground based instruments for observing GCRs, as for example Water Cherenkov Detectors (e.g., Santos, Dasso, Gulisano, Areso, Pereira, Asorey, Rubinstein and LAGO Collaboration, 2023).

Acknowledgements

We thank the referees for their comments which improved the manuscript. C.G. is fellow of CONICET. S.D. is a member of the Carrera del Investigador Científico, CONICET. This work was supported by the Argentinean grants PICT 2019-02754 (FONCyT-ANPCyT) and UBACyT-200-20190100247BA (UBA). S.D. thanks the LIA project (LIA-1208). This work was supported by a one-month invitation of S.D. to Paris Observatory. We acknowledge the NMDB database www.nmdb.eu, founded under the European Union's FP7 programme (contract no. 213007) for providing data. The neutron monitor data from McMurdo are provided by the University of Delaware Department of Physics and Astronomy and the Bartol Research Institute. We thank the ACE SWEPAM and MAG instruments teams and the ACE Science Center for providing the ACE data. We recognize the collaborative and open nature of knowledge creation and dissemination, under the control of the academic community as expressed by Camille Noûs at <http://www.cogitamus.fr/indexen.html>.

References

- Badruddin, 1996. Cosmic Ray Modulation: Effects Of High Speed Solar Wind Streams. *Astrophys. Spa. Sci.* 246, 171–191. doi:10.1007/BF00645638.
- Badruddin, Kumar, A., 2016. Study of the Cosmic-Ray Modulation During the Passage of ICMEs and CIRs. *Solar Phys.* 291, 559–580. doi:10.1007/s11207-015-0843-4.
- Badruddin, Venkatesan, D., Zhu, B.Y., 1991. Study and Effect of Magnetic Clouds on the Transient Modulation of Cosmic-Ray Intensity. *Solar Phys.* 134, 203–209. doi:10.1007/BF00148748.
- Badruddin, Yadav, R.S., Yadav, N.R., 1986. Influence of Magnetic Clouds on Cosmic-Ray Intensity Variation. *Solar Phys.* 105, 413–428. doi:10.1007/BF00172057.
- Badruddin, A., Falak, Z., 2016. Study of the geoeffectiveness of coronal mass ejections, corotating interaction regions and their associated structures observed during Solar Cycle 23. *Astrophys. Spa. Sci.* 361, 253. doi:10.1007/s10509-016-2839-4.
- Belov, A., Abunin, A., Abunina, M., Eroshenko, E., Oleneva, V., Yanke, V., Papaioannou, A., Mavromichalaki, H., 2015. Galactic Cosmic Ray Density Variations in Magnetic Clouds. *Solar Phys.* 290, 1429–1444. doi:10.1007/s11207-015-0678-z.
- Burlaga, L., Sittler, E., Mariani, F., Schwenn, R., 1981. Magnetic loop behind an interplanetary shock: Voyager, Helios, and IMP 8 observations. *J. Geophys. Res.* 86, 6673–6684. doi:10.1029/JA086iA08p06673.
- Cane, H.V., 2000. Coronal Mass Ejections and Forbush Decreases. *Space Sci. Rev.* 93, 55–77. doi:10.1023/A:1026532125747.
- Chree, C., 1913. Some Phenomena of Sunspots and of Terrestrial Magnetism at Kew Observatory. *Philosophical Transactions of the Royal Society of London Series A* 212, 75–116. doi:10.1098/rsta.1913.0003.
- Dasso, S., Mandrini, C.H., Démoulin, P., Luoni, M.L., Gulisano, A.M., 2005. Large scale MHD properties of interplanetary magnetic clouds. *Adv. Spa. Res.* 35, 711–724. doi:10.1016/j.asr.2005.02.096.
- Démoulin, P., 2009. Why Do Temperature and Velocity Have Different Relationships in the Solar Wind and in Interplanetary Coronal Mass Ejections? *Solar Phys.* 257, 169–184. doi:10.1007/s11207-009-9338-5.
- Démoulin, P., Dasso, S., 2009. Causes and consequences of magnetic cloud expansion. *Astron. Astrophys.* 498, 551–566. doi:10.1051/0004-6361/200810971.
- Démoulin, P., Nakwacki, M.S., Dasso, S., Mandrini, C.H., 2008. Expected in Situ Velocities from a Hierarchical Model for Expanding Interplanetary Coronal Mass Ejections. *Solar Phys.* 250, 347–374. doi:10.1007/s11207-008-9221-9.
- Dumbović, M., Vršnak, B., Guo, J., Heber, B., Dissauer, K., Carcaboso, F., Temmer, M., Veronig, A., Podladchikova, T., Möstl, C., Amerstorfer, T., Kirin, A., 2020. Evolution of Coronal Mass Ejections and the Corresponding Forbush Decreases: Modeling vs. Multi-Spacecraft Observations. *Solar Phys.* 295, 104. doi:10.1007/s11207-020-01671-7, arXiv:2006.02253.
- Dumbović, M., Vršnak, B., Temmer, M., Heber, B., Kühl, P., 2022. Generic profile of a long-lived corotating interaction region and associated recurrent Forbush decrease. *Astron. Astrophys.* 658, A187. doi:10.1051/0004-6361/202140861, arXiv:2201.09623.
- Dumbović, M., Vršnak, B., Čalogović, J., Karlica, M., 2011. Cosmic ray modulation by solar wind disturbances. *Astron. Astrophys.* 531, A91. doi:10.1051/0004-6361/201016006.
- Elliott, H.A., Henney, C.J., McComas, D.J., Smith, C.W., Vasquez, B.J., 2012. Temporal and radial variation of the solar wind temperature-speed relationship. *Journal of Geophysical Research (Space Physics)* 117, A09102. doi:10.1029/2011JA017125.
- Forbush, S.E., 1937. On the Effects in Cosmic-Ray Intensity Observed During the Recent Magnetic Storm. *Physical Review* 51, 1108–1109. doi:10.1103/PhysRev.51.1108.3.
- Gosling, J.T., Borrini, G., Asbridge, J.R., Bame, S.J., Feldman, W.C., Hansen, R.T., 1981. Coronal streamers in the solar wind at 1 AU. *J. Geophys. Res.* 86, 5438–5448. doi:10.1029/JA086iA07p05438.
- Gutierrez, C., Dasso, S., 2021. Modulación interplanetaria del flujo de rayos cósmicos galácticos. *Boletín de la Asociación Argentina de Astronomía La Plata Argentina* 62, 13–15.
- Hess, V.F., Demmelair, A., 1937. World-wide Effect in Cosmic Ray Intensity, as Observed during a Recent Magnetic Storm. *Nature* 140, 316–317. doi:10.1038/140316a0.
- Janvier, M., Démoulin, P., Guo, J., Dasso, S., Regnault, F., Topsis-Moutesidou, S., Gutierrez, C., Perri, B., 2021. The Two-step Forbush Decrease: A Tale of Two Substructures Modulating Galactic Cosmic Rays within Coronal Mass Ejections. *Astrophys. J.* 922, 216. doi:10.3847/1538-4357/ac2b9b, arXiv:2109.14469.
- Jian, L., Russell, C.T., Luhmann, J.G., Skoug, R.M., 2006. Properties of Stream Interactions at One AU During 1995–2004. *Solar Phys.* 239, 337–392. doi:10.1007/s11207-006-0132-3.
- Kharayat, H., Prasad, L., Mathpal, R., Garia, S., Bhatt, B., 2016. Study of Cosmic Ray Intensity in Relation to the Interplanetary Magnetic Field and Geomagnetic Storms for Solar Cycle 23. *Solar Phys.* 291, 603–611. doi:10.1007/s11207-016-0852-y.
- Kilpua, E., Koskinen, H.E.J., Pulkkinen, T.I., 2017. Coronal mass ejections and their sheath regions in interplanetary space. *Living Reviews in Solar Physics* 14, 5. doi:10.1007/s41116-017-0009-6.
- Klein, L.W., Burlaga, L.F., 1982. Interplanetary magnetic clouds at 1 AU. *J. Geophys. Res.* 87, 613–624. doi:10.1029/JA087iA02p0613.
- Krieger, A.S., Timothy, A.F., Roelof, E.C., 1973. A Coronal Hole and Its Identification as the Source of a High Velocity Solar Wind Stream. *Solar Phys.* 29, 505–525. doi:10.1007/BF00150828.
- Lanabere, V., Dasso, S., Démoulin, P., Janvier, M., Rodriguez, L., Masías-Meza, J.J., 2020. Magnetic twist profile inside magnetic clouds derived with a superposed epoch analysis. *Astron. Astrophys.* 635, A85. doi:10.

- 1051/0004-6361/201937404, arXiv:2002.10606.
- Lanabere, V., Démoulin, P., Dasso, S., 2022. A robust estimation of the twist distribution in magnetic clouds. *Astron. Astrophys.* 668, A160. doi:10.1051/0004-6361/202245062, arXiv:2211.08758.
- Lepping, R.P., Berdichevsky, D.B., Szabo, A., Arqueros, C., Lazarus, A.J., 2003. Profile of an Average Magnetic Cloud at 1 au for the Quiet Solar Phase: Wind Observations. *Solar Phys.* 212, 425–444. doi:10.1023/A:1022938903870.
- Lockwood, J.A., 1971. Forbush Decreases in the Cosmic Radiation. *Space Sci. Rev.* 12, 658–715. doi:10.1007/BF00173346.
- Lopez, R.E., Freeman, J.W., 1986. Solar wind proton temperature-velocity relationship. *J. Geophys. Res.* 91, 1701–1705. doi:10.1029/JA091iA02p01701.
- Masías-Meza, J.J., Dasso, S., Démoulin, P., Rodriguez, L., Janvier, M., 2016. Superposed epoch study of ICME sub-structures near Earth and their effects on Galactic cosmic rays. *Astron. Astrophys.* 592, A118. doi:10.1051/0004-6361/201628571, arXiv:1605.08130.
- McComas, D.J., Bame, S.J., Barker, P., Feldman, W.C., Phillips, J.L., Riley, P., Griffee, J.W., 1998. Solar Wind Electron Proton Alpha Monitor (SWEPAM) for the Advanced Composition Explorer. *Space Sci. Rev.* 86, 563–612. doi:10.1023/A:1005040232597.
- Melkumyan, A.A., Belov, A.V., Abunina, M.A., Abunin, A.A., Eroshenko, E.A., Yanke, V.G., Oleneva, V.A., 2019. Comparison between statistical properties of Forbush decreases caused by solar wind disturbances from coronal mass ejections and coronal holes. *Advances in Space Research* 63, 1100–1109. doi:10.1016/j.asr.2018.10.009.
- Melkumyan, A.A., Belov, A.V., Shlyk, N.S., Abunina, M.A., Abunin, A.A., Oleneva, V.A., Yanke, V.G., 2023. Statistical comparison of time profiles of Forbush decreases associated with coronal mass ejections and streams from coronal holes in solar cycles 23-24. *Mon. Not. Roy. Astron. Soc.* 521, 4544–4560. doi:10.1093/mnras/stad772.
- Parker, E.N., 1965. The passage of energetic charged particles through interplanetary space. *Planetary Spa. Sci.* 13, 9–49. doi:10.1016/0032-0633(65)90131-5.
- Raghav, A., Shaikh, Z., Misal, D., Rajan, G., Mishra, W., Kasthurirangan, S., Bhaskar, A., Bijewar, N., Johri, A., Vichare, G., 2020. Exploring the common origins of the Forbush decrease phenomenon caused by the interplanetary counterpart of coronal mass ejections or corotating interaction regions. *Physical Review D* 101, 062003. doi:10.1103/PhysRevD.101.062003.
- Regnault, F., Janvier, M., Démoulin, P., Auchère, F., Strugarek, A., Dasso, S., Noûs, C., 2020. 20 Years of ACE Data: How Superposed Epoch Analyses Reveal Generic Features in Interplanetary CME Profiles. *Journal of Geophysical Research (Space Physics)* 125, e28150. doi:10.1029/2020JA028150, arXiv:2011.05050.
- Richardson, I.G., 2004. Energetic Particles and Corotating Interaction Regions in the Solar Wind. *Space Sci. Rev.* 111, 267–376. doi:10.1023/B:SPAC.0000032689.52830.3e.
- Richardson, I.G., 2018. Solar wind stream interaction regions throughout the heliosphere. *Living Reviews in Solar Physics* 15, 1. doi:10.1007/s41116-017-0011-z.
- Richardson, I.G., Cane, H.V., 2010. Near-Earth Interplanetary Coronal Mass Ejections During Solar Cycle 23 (1996 - 2009): Catalog and Summary of Properties. *Solar Phys.* 264, 189–237. doi:10.1007/s11207-010-9568-6.
- Richardson, I.G., Wibberenz, G., Cane, H.V., 1996. The relationship between recurring cosmic ray depressions and corotating solar wind streams at ≤ 1 AU: IMP 8 and Helios 1 and 2 anticoincidence guard rate observations. *J. Geophys. Res.* 101, 13483–13496. doi:10.1029/96JA00547.
- Rodriguez, L., Masías-Meza, J.J., Dasso, S., Démoulin, P., Zhukov, A.N., Gulisano, A.M., Mierla, M., Kilpua, E., West, M., Lacatus, D., Paraschiv, A., Janvier, M., 2016. Typical Profiles and Distributions of Plasma and Magnetic Field Parameters in Magnetic Clouds at 1 AU. *Solar Phys.* 291, 2145–2163. doi:10.1007/s11207-016-0955-5.
- Rouillard, A.P., 2011. Relating white light and in situ observations of coronal mass ejections: A review. *Journal of Atmospheric and Solar-Terrestrial Physics* 73, 1201–1213. doi:10.1016/j.jastp.2010.08.015.
- Russell, C.T., Mulligan, T., 2002. On the magnetosheath thicknesses of interplanetary coronal mass ejections. *Planetary Spa. Sci.* 50, 527–534. doi:10.1016/S0032-0633(02)00031-4.
- Santos, N.A., Dasso, S., Gulisano, A.M., Areso, O., Pereira, M., Asorey, H., Rubinstein, L., LAGO Collaboration, 2023. First measurements of periodicities and anisotropies of cosmic ray flux observed with a water-Cherenkov detector at the Marambio Antarctic base. *Advances in Space Research* 71, 2967–2976. doi:10.1016/j.asr.2022.11.041.
- Simpson, J.A., 1998. A Brief History of Recurrent Solar Modulation of the Galactic Cosmic Rays (1937-1990). *Space Sci. Rev.* 83, 169–176.
- Simpson, J.A., 2000. The Cosmic Ray Nucleonic Component: The Invention and Scientific Uses of the Neutron Monitor - (Keynote Lecture). *Space Sci. Rev.* 93, 11–32. doi:10.1023/A:1026567706183.
- Smith, C.W., L'Heureux, J., Ness, N.F., Acuña, M.H., Burlaga, L.F., Scheifele, J., 1998. The ACE Magnetic Fields Experiment. *Space Sci. Rev.* 86, 613–632. doi:10.1023/A:1005092216668.
- Stone, E.C., Frandsen, A.M., Mewaldt, R.A., Christian, E.R., Margolies, D., Ormes, J.F., Snow, F., 1998. The Advanced Composition Explorer. *Space Sci. Rev.* 86, 1–22. doi:10.1023/A:1005082526237.
- Usoskin, I.G., Kananen, H., Mursula, K., Tanskanen, P., Kovaltsov, G.A., 1998. Correlative study of solar activity and cosmic ray intensity. *J. Geophys. Res.* 103, 9567–9574. doi:10.1029/97JA03782.